

## Atmosphere and Annealing Effect on the Structural, Optical and Electrical Properties of Indium Tin Oxide

<sup>1</sup>Ehssan S. Hassan, <sup>1</sup>Wisam J. Aziz, <sup>2</sup>Ahmed Naji. Abd, <sup>1</sup>Mohamed Odda Dawod and <sup>2</sup>Nadir Fadhil Habubi  
<sup>1</sup>Department of Physics, Faculty of Science, Mustansiriyah University, Baghdad, Iraq  
<sup>2</sup>Department of Physics, Faculty of Education, Mustansiriyah University, Baghdad, Iraq

**Abstract:** Indium-doped tin oxide  $\text{In}_2\text{Sn}_2\text{O}_7$  thin films were deposited on Superior w. Germany glass substrate by RF magnetron sputtering technique using a popular ceramic target with a combination of In 8 wt.% and  $\text{SnO}_2$  at a working pressure of  $4.2 \times 10^{-3}$  torr and radio frequency power of 100 W. These films were post-annealed at temperatures from 200-400°C for 1 h by both oxygen atmosphere and vacuum furnace. The resulting films were studied by X-ray diffraction reveals a poly crystalline structure of  $\text{In}_2\text{Sn}_2\text{O}_7$  phase formation with diffraction peaks related to the cubic phase structure of  $\text{In}_2\text{Sn}_2\text{O}_7$  according to JCPDS card 391058. The post-annealing atmospheric effects on micro structural, electrical and optical properties of  $\text{In}_2\text{Sn}_2\text{O}_7$  films were determined. The results assure that at a higher annealing temperature, the crystallinity of  $\text{In}_2\text{Sn}_2\text{O}_7$  films was enhanced, the optical transmittance of  $\text{In}_2\text{Sn}_2\text{O}_7$  thin films was increased over 90% at 650 nm in the oxygen atmosphere, compared to 85% at 680 nm for the same annealing temperature in the vacuum atmosphere. The resistivity of  $\text{In}_2\text{Sn}_2\text{O}_7$  thin films was increased with advanced annealing temperatures in the both vacuum and oxygen atmosphere furnace.

**Key words:** Indium-doped tin oxide, transitional conductive oxide, radio frequency magnetron sputtering, annealing atmosphere and transmittance, cubic phase, enhanced

---

### INTRODUCTION

Transparent Conducting Oxide TCO has been generally used as a transparent conducting thin film material that entered in numerous fields such as solar cells, optoelectronic devices, heatmirrors and gas sensor (Jun *et al.*, 2006). The high significance of many transparent conductors has accelerated the expansion of cheap TCO materials. Indium-doped Tin Oxide ITO films were fine recognized for TCO resources because of its tremendous electrical and optical properties (Harrison and Willett, 1988). However, its high treating cost is a weakness. ZnO film is less expensive than Indium Tin Oxide ITO but it shows low thermal strength. In comparing ITO films with the  $\text{SnO}_2$  film, ITO shows the best thermal and chemical stability.  $\text{SnO}_2$  is n-type semi conductor with a variable value of the band gap of nearly 3.7 eV. Pure  $\text{SnO}_2$  films are low electrical conductors that are greatly transparent in the visible range. Conversely, their low electrical conductivity can be enhanced by governing stoichiometry or doping with impurities. The electrical conductivity of indium-doped tin oxide films are set by various systems such as Chemical Vapor Deposition CVD (Abbet and Heiz, 2005) spray pyrolysis

(Kroes *et al.*, 2002) sputtering and evaporation (Alivisatos, 1996) construction on the potential of RF technique (Na *et al.*, 2009). It has been established that doping  $\text{SnO}_2$  with Sb improves both electrical conductivity and transitions which can be attributed to the increase in the density of free charge carriers. Also, ITO, zinc oxide and tin oxide  $\text{SnO}_2$  are the three greatest main TCOs and are previously broadly used as thin film solar cells (Huang and El-Sayed, 2010). In addition, aluminum-doped zinc oxide and Fluorine-doped Tin Oxide FTO is among the other most dominant TCOs in numerous technological fields, mainly the optoelectronic device industry where TCOs have proved essential for applications such as photo electro chemical devices, light emitting diodes, liquid crystal displays and gas sensors (Cui *et al.*, 2006). ITO's can be set by direct current DC and Radio Frequency (RF) magnetron sputtering, electron beam evaporation, thermal vapor evaporation, spray pyrolysis, chemical solution deposition and sol-gel methods (Arruebo *et al.*, 2007). Radio frequency magnetron sputtering can be used by governed the electrical and optical properties of ITO thin films and are greatly used in the manufacture (Cheng *et al.*, 2006). Gheidari *et al.* (2007) was focused on

the effect of the sputtering pressure and annealing temperature on the properties of ITO films. They found that the deposition rate decreases above 30 m torr and the best conductivity and transmittance and larger grain size were achieved with an annealing temperature of 400°C (Gheidari *et al.*, 2007). Li *et al.* (2007) declared that the annealing process may effectively improve the film performance. Chang *et al.* (2001) studied the effect of post annealing for doped ZnO. This study is seeking to further understand the effect of oxygen concentration on the properties of ITO thin films and the influence on its quality.

### MATERIALS AND METHODS

The sputtered target was a mixture of high purity 99.99% indium metal of 8 wt.% and SnO<sub>2</sub> 92 W% high purity 99.998% Merck Germany and the films were deposited on a glass substrate Superior w. Germany by RF-magnetron sputter system torr international in C.CRC 600. The films were separately annealed in vacuum furnace at a pressure of 1 m torr and oxygen atmosphere furnace with extending temperatures from 200-400°C for 1 h. The effect of after deposition annealing atmosphere on micro structural, electrical and optical properties of the ITO films was studied. The sputtering space was emptied to a pressure of  $7.4 \times 10^{-6}$  torr by the combination of oil pump, rotary and turbo molecular pump before plasma producing, the deposition power was fixed at 150 W at a frequency of 13.56 MHz. The angle between the electrodes and the substrate point was 45° and the distance between the target and the glass substrate was 10 cm. The drift rate of argon gas was immobile to 30 sccm by the Ailcat mass flow controller. ITO film was deposited at an employed pressure of  $1 \times 10^{-3}$  torr and radio frequency power of 100W. The surface microstructure was examined by S-4160-Hitachi (College of Engineering and Communications, Iran Tehran) Scanning Electron Microscopy SEM. The microstructure of the film was characterized by a Shimadzu 6-2006 with CuK<sub>α</sub> radiation having wavelength  $\lambda = 0.15406$  nm. The Hall mobility and the carrier concentration of these films were examined by Hall measurement system model ECOPIA, HMS-3000. The optical transmittance of thin films was observed using a Cary 100 conc UV-Visible spectroscopy spectrophotometer in the visible range of wavelengths (400-800 nm).

### RESULTS AND DISCUSSION

The XRD spectra of In<sub>2</sub>Sn<sub>2</sub>O<sub>7</sub> films prepared by radio frequency magnetron sputtering and post-annealing temperatures (200, 300 and 400°C) onto glass substrates depicts by Fig. 1 which shows the samples that annealed

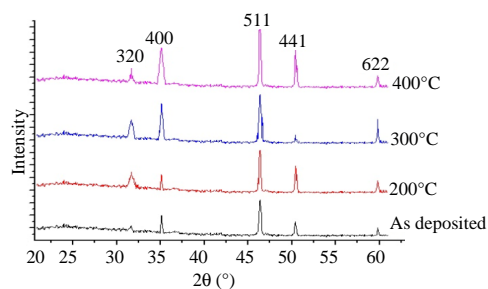


Fig. 1: (XRD) patterns of the ITO films as-deposited and annealed at vacuum atmospheres

in vacuum furnace. The In<sub>2</sub>Sn<sub>2</sub>O<sub>7</sub> deposited films were poly crystalline cubic structure with diffraction peaks related to the JCPDS card no. 391058 (Marikkannan *et al.*, 2015). From this figure, it can be seen that the major peak was (511) plane and corresponds to  $2\theta = 46.45^\circ$  and minor small peaks (320), (400), (622) and (441) planes were observed. From these patterns, it is perceptible that as the annealing temperature increased, the intensities of the peaks were improved which is due to the sufficient increase in the supply of thermal energy for crystallization (Ashida *et al.*, 2009). The average crystallite size (D) of all prepared samples with different annealing temperatures have been calculated using the Debye-Scherrer's Eq. 1 (Algar *et al.*, 2012):

$$D = \frac{0.9\lambda}{\beta \cos\theta} \quad (1)$$

Where:

$\beta$  = The full width at half maximum

$\theta$  = The Bragg's angle

It can be noticed that the crystallite size increased with increasing the annealing temperature, up to 400°C, due to the chemical adsorption of oxygen on the surface of film (Spinelli *et al.*, 2012). In the oxygen atmosphere furnace as shown in Fig. 2 in spite of varying the oxygen concentrations, there is no change in the preferred orientation (511) plane of the films. The annealing temperature increased, the crystallite size gets smaller because of a decrease in the order of crystallinity of the film which also, caused the increase in the FWHM of the (511) plane (Zaier *et al.*, 2015). As the annealing temperature increasing from (300-400°C) the intensity increases which are strongly dependent on the critical level of In<sup>+3</sup> and O<sup>-2</sup> pairs and the pair's density were different for different annealing time (Vora *et al.*, 2014). While a further increase in the annealing temperature to 400°C led to enhanced order of crystallinity due to the film growth from the initial nuclei, the crystal plane of the

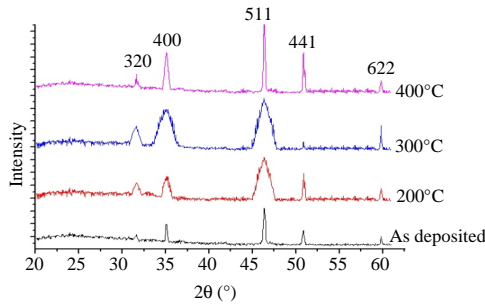


Fig. 2: (XRD) patterns of the ITO films as-deposited and annealed at oxygen atmospheres

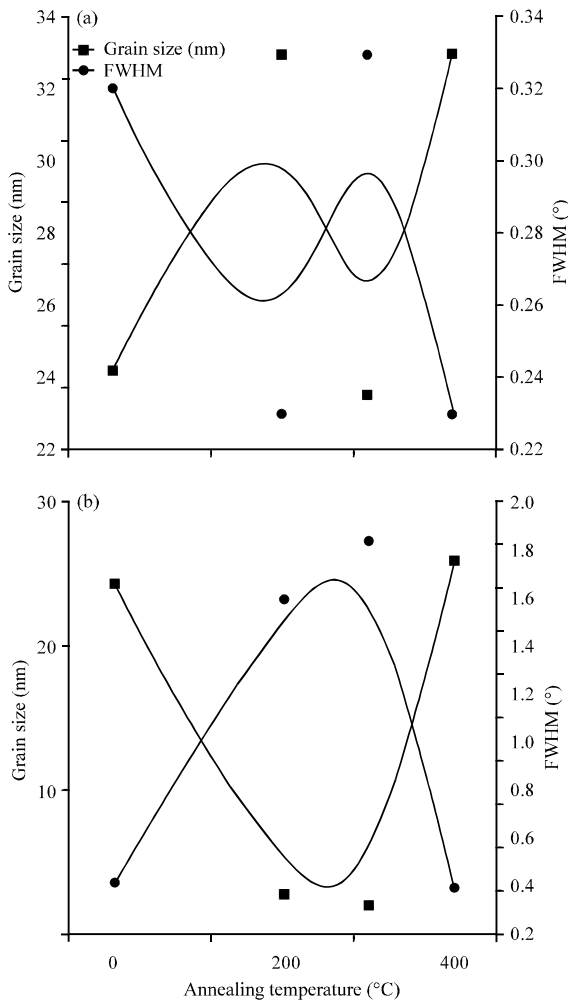


Fig. 3: Crystallite size and FWHM of the ITO films annealed in; a) Avacuum atmosphere and b) Oxygen atmosphere

nuclei with minimum surface free energy may remain parallel to the film surface because the growth rate of the crystal plane with minimum surface free energy is lower than the other crystal plane (Gwamuri *et al.*, 2016).

Figure 3 shows the crystallite size and the FWHM as function of annealing temperature in both vacuum and oxygen furnace.

**Morphological analysis:** The  $\text{In}_2\text{Sn}_2\text{O}_7$  nano films prepared by RF magnetron sputtering process were characterized by SEM images. It has been observed that the change in annealing temperature contributes to a large variation in the morphology of nanostructures. In this research, the annealing temperatures were (200-400°C) in both oxygen and vacuum atmosphere. Figure 4b-d shows typical SEM images of the preparation  $\text{In}_2\text{Sn}_2\text{O}_7$  nanostructures at different annealing temperature (200-400°C) in the vacuum atmosphere. The dominant structures obtained from the Fig. 4b where nanoparticles with a diameter of 40 nm, the inset Fig. 4b represents a closer look of the film surface. When the temperature increased to 300°C, nanorods with a diameter of 50 nm can be observed as in the inset Fig. 4c. When the reaction temperature is further increased to 400°C, a large scale nanoparticles were observed as in Fig. 4d. The inset in Fig. 4d represents the cross section view of the nanorod structure of  $\text{In}_2\text{Sn}_2\text{O}_7$ . These results could be described to the increased in the annealing temperature which led to improved crystalline growth to be faster upward in the direction of the film growth and faster radially outward relative to the surrounding amorphous material. The upward growth rate is approximately 20% faster than the growth rate of the amorphous material. At higher deposition temperatures, nucleation events become more probable and thus, the film becomes more crystalline. As the film grows thicker, the total number of nuclei increase and the films become more crystalline due to the growth of the nuclei crystallinity. At some point during the deposition process the surface becomes saturated with crystallites and further nucleation events and radial crystal growth will cease. However, vertical growth in the direction of the growing film will continue and crystallites will begin to assume a columnar structure (Hausmann and Gordon, 2003). The upper the annealing temperature, the improved in order of crystallinity and the crystallinity of the deposited  $\text{In}_2\text{Sn}_2\text{O}_7$  film enhanced and causes less shallow scattering of charge carriers (Vink *et al.*, 1995). Figure 4e-h which shows the SEM image of the vacuum samples during the annealing process with the exposure of  $\text{O}_2$  indium as a reactant captured  $\text{O}_2$  to form  $\text{In}_2\text{O}_3$  nuclei to assure the annealing of the nanoparticle. Nanoparticle would grow along three directions one of these directions would be tenthly especially but shorter along the other two directions. The dominant structures obtained from the Fig. 4e where nanoparticles with diameters of 30 nm. When the

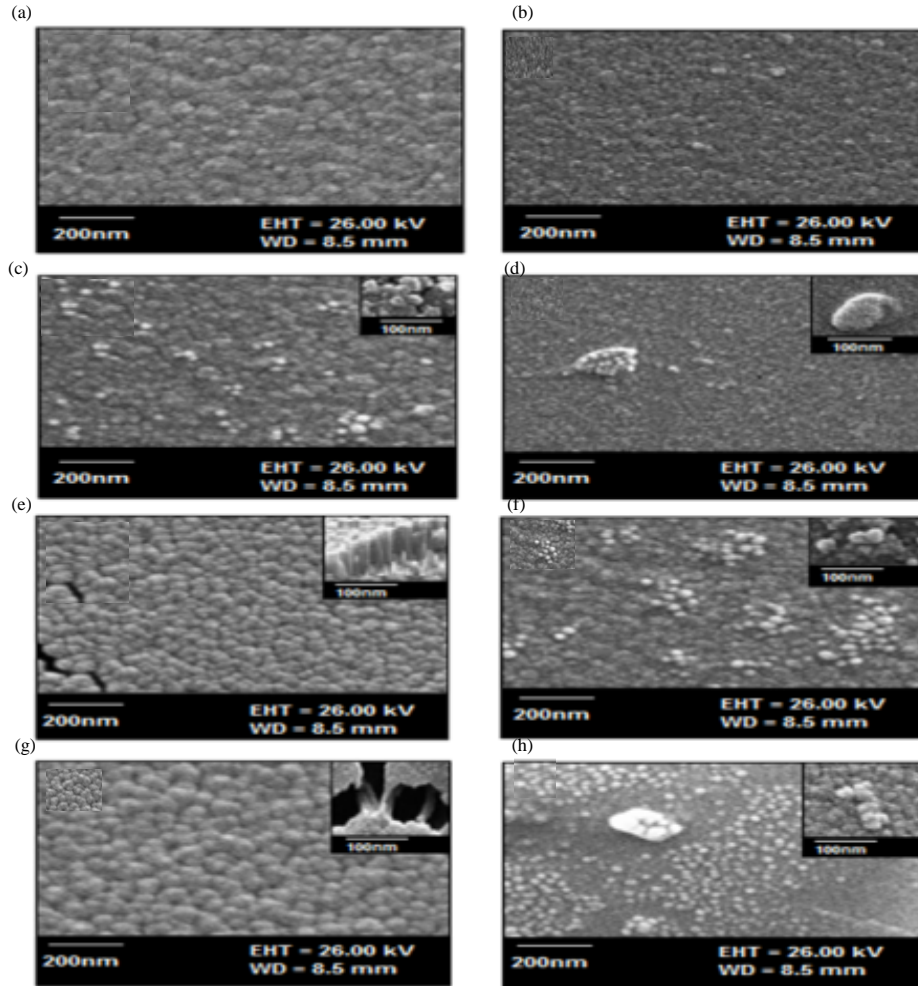


Fig. 4: Scanning electron micrographs of the  $\text{In}_2\text{Sn}_2\text{O}_7$  films; a) As-deposited; b-d) annealed in a vacuum atmosphere at (200-400) $^\circ\text{C}$  and e-h) annealed in oxygen atmosphere at (200-400) $^\circ\text{C}$

temperature increased to 300 $^\circ\text{C}$ , nanoparticles with a diameter of 15 nm can be observed as in Fig. 4g. When the reaction temperature is further increased to 400 $^\circ\text{C}$  a larger scale nanoparticles were observed as in Fig. 4h, the inset figure in the Fig. 4h shows the 100 nm scale image.

**Transmission:** The optical transmittance of  $\text{In}_2\text{Sn}_2\text{O}_7$  films deposited on glass prepared by RF sputtering technique was measured by UV-Vis spectrophotometer. Figure 5a shows the transmittance via wavelengths of the films deposited at numerous temperatures from (200-400 $^\circ\text{C}$ ) in a vacuum which reveal that the transmittance was governed by the temperature. It was established that the average transmittance of the

$\text{In}_2\text{Sn}_2\text{O}_7$  film outdied 85% in the visible region. For all the studied films, it was seen that the optical transmittance decreases marginally with increasing the substrate temperature. This can attribute to the increase of surface roughness promoting the increase of the surface scattering of the light. Figure 5b shows the optical transmittance of the  $\text{In}_2\text{Sn}_2\text{O}_7$  films, annealed in the oxygen atmosphere and deposited on a glass substrate. It was found that the optical transmission of the  $\text{In}_2\text{Sn}_2\text{O}_7$  films at oxide atmosphere is 90% and it was higher than that of vacuum atmosphere. The transmittance value decreases with annealing temperature increasing up to the highest annealing temperature, this indicates that the decreases in optical transmission with increasing annealing temperature might be due to an increase of surface roughness.

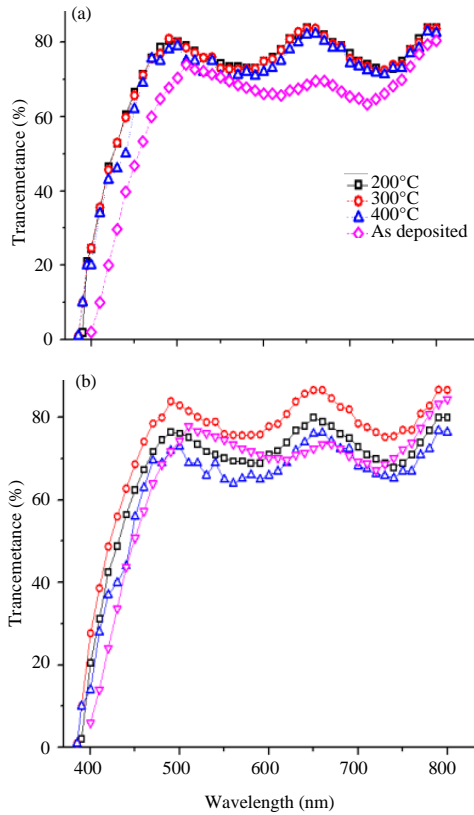


Fig. 5: Optical transmittance of the ITO films annealed at different annealing temperature and atmospheres; a) Vacuum atmosphere and b) Oxygen atmosphere

**Resistivity:** Figure 6 shows the resistivity, Hall coefficient and charge carrier concentration of the  $\text{In}_2\text{Sn}_2\text{O}_7$  films annealed at a different annealing temperatures in different annealing atmospheres. It can be seen that the electrical resistivity of  $\text{In}_2\text{Sn}_2\text{O}_7$  films was obviously influenced by the annealing temperature and at various atmospheres as the annealing temperature rises from (200-300°C), the resistivity of the ITO films obviously increases from (7.32-8.91 kΩ.cm) when annealed in a vacuum atmosphere, farther the temperature increasing to 400° C, the resistivity drops to 4.66 kΩ.cm. Many earlier studies illustrated that the higher annealing temperature in vacuity caused subordinate resistivity (Luo *et al.*, 2006; Vora *et al.*, 2014). The decrease in electrical resistivity with rising annealing temperature led to improved the crystallinity of films. Also, the Hall mobility and carrier concentration were evaluated and show generally increases with the temperature increasing as shown in Fig. 6a while the investigating of the resistivity, Hall mobility and

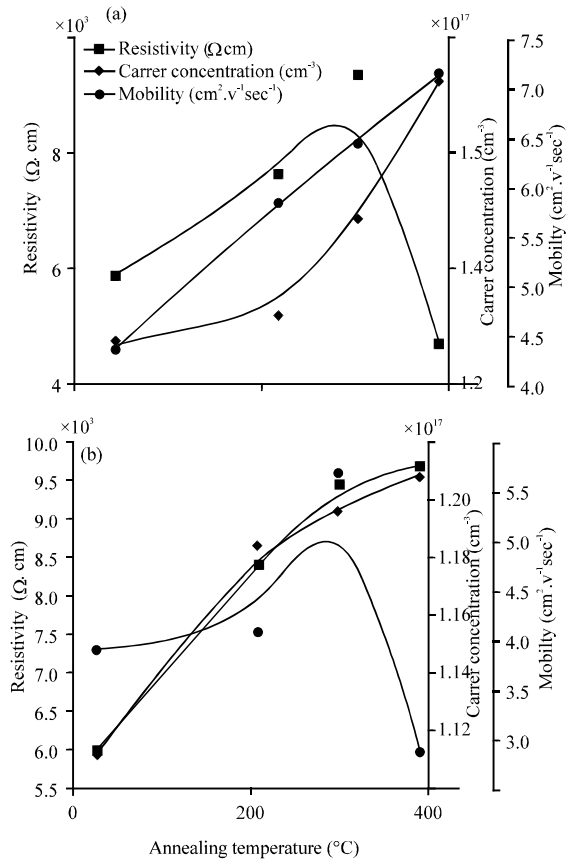


Fig. 6: Resistivity of the ITO films annealed at different temperature and atmospheres: a) In avacuumatmosphere and b) In oxygen atmosphere

charge carrier concentration in oxidizing atmosphere shows continuously increasing in the resistivity from (6-9.62 kΩ.cm) as the annealing temperature rise from (200-400°C). This consequence improved resistivity, due to the oxygen positions and interstitial Sn atoms that acted as donors, giving growth to advanced carrier concentration and Hall mobility (Zeng *et al.*, 2008). Furthermore, the surface mobility was better with rising annealing temperature and thus, the crystalline size became larger.

### CONCLUSION

The structural characteristics change as can be seen that the crystallite size in the vacuum atmosphere is constantly increasing when the annealing temperature increases while it is decreases and then increases in the oxygen atmosphere. The vertical growth of the nanorods which increases the roughness of the surface while

increasing the temperature in the vacuum or oxygen medium and the transmission of the oxygen atmosphere is higher than the vacuum atmosphere by 10% and that the transmission decreased with the increase in annealing temperature. It is noted that the electrical resistance of the oxygen atmosphere is increasing from (6-6.92 k $\Omega$ .cm) As the annealing temperature increasing and it is higher than of the vacuum atmosphere which decreases from (7.32-4.66 k $\Omega$ .cm) as the annealing temperature increased.

#### ACKNOWLEDGEMENTS

This study was supported by the Mustansiriyah University, College of Science and College of Education, Physics Department and the teamwork would like to thank the Ministry of Science and Technology for providing support through the RF-magnetron sputtering system and furnace vacuum.

#### REFERENCES

- Abbet, S. and U. Heiz, 2005. Nanocatalysis. Wiley-VCH Verlag GmbH & Co., KGaA, Weinheim, Germany.
- Algar, M., T.Theivasanthi and A.K. Raja, 2012. Chemical synthesis of nano-sized particles of lead oxide and their characterization studies. J. Applied Sci., 12: 398-401.
- Alivisatos, A.P., 1996. Semiconductor clusters, nanocrystals and quantum dots. Science, 271: 933-937.
- Arruebo, M., R. Fernandez-Pacheco, M.R. Ibarra and J. Santamaria, 2007. Magnetic nanoparticles for drug delivery. Nano Today, 2: 22-32.
- Ashida, T., A. Miyamura, N. Oka, Y. Sato and T. Yagi *et al.*, 2009. Thermal transport properties of polycrystalline tin-doped indium oxide films. J. Appl. Phys., 105: 073709-073712.
- Chang, J.F., W.C. Lin and M.H. Hon, 2001. Effects of post-annealing on the structure and properties of Al-doped Zinc Oxide films. Appl. Surf. Sci., 183: 18-25.
- Cheng, G., E. Stern, S. Guthrie, M.A. Reed and R. Klie, *et al.*, 2006. Indium oxide nanostructures. Appl. Phys. A., 85: 233-240.
- Cui, H., P. Liu and G.W. Yang, 2006. Noble metal nanoparticle patterning deposition using pulsed-laser deposition in liquid for surface-enhanced Raman scattering. Appl. Phys. Lett., 89: 124-153.
- Gheidari, A.M., F. Behafarid, G. Kavei and M. Kazemzad, 2007. Effect of sputtering pressure and annealing temperature on the properties of indium tin oxide thin films. Mater. Sci. Eng. B., 136: 37-40.
- Gwamuri, J., A. Vora, J. Mayandi, D.O. Guney and P.L. Bergstrom *et al.*, 2016. A new method of preparing highly conductive ultra-thin indium tin oxide for plasmonic-enhanced thin film solar photovoltaic devices. Solar Energy Mater. Cells, 149: 250-257.
- Harrison, P.G. and M.J. Willett, 1988. The mechanism of operation of tin (IV) oxide carbon monoxide sensors. Nat., 332: 337-339.
- Hausmann, D.M. and R.G. Gordon, 2003. Surface morphology and crystallinity control in the Atomic Layer Deposition (ALD) of hafnium and Zirconium Oxide thin films. J. Cryst. Growth, 249: 251-261.
- Huang, X. and M.A. El-Sayed, 2010. Gold nanoparticles: Optical properties and implementations in cancer diagnosis and photothermal therapy. J. Adv. Res., 1: 13-28.
- Jun, Y.W., J.S. Choi and J. Cheon, 2006. Shape control of semiconductor and metal oxide nanocrystals through nonhydrolytic colloidal routes. Angew. Chem. Intl. Ed., 45: 3414-3439.
- Kroes, G.J., A. Gross, E.J. Baerends, M. Scheffler and D.A. McCormack, 2002. Quantum theory of dissociative chemisorption on metal surfaces. Acc. Chem. Res., 35: 193-200.
- Li, L., L. Fang, X. Chen, G. Liu and J. Liu *et al.*, 2007. Effect of annealing treatment on the structural, optical and electrical properties of Al-doped ZnO thin films. Rare Met., 26: 247-253.
- Luo, S.N., A. Kono, N. Nouchi and F. Shoji, 2006. Effective creation of oxygen vacancies as an electron carrier source in tin-doped indium oxide films by plasma sputtering. J. Appl. Phys., 100: 113701-113709.
- Marikkannan, M., M. Subramanian, J. Mayandi, M. Tanemura and V. Vishnukanthan *et al.*, 2015. Effect of ambient combinations of Argon, Oxygen and Hydrogen on the properties of DC magnetron sputtered indium tin oxide films. AIP Adva., 5: 1-13.
- Na, H.B., I.C. Song and T. Hyeon, 2009. Inorganic nanoparticles for MRI contrast agents. Adv. Mater., 21: 2133-2148.
- Spinelli, P., V.E. Ferry, J. Van De Groep, M. Van Lare and M.A. Verschuuren *et al.*, 2012. Plasmonic light trapping in thin-film Si solar cells. J. Opt., 14: 1-11.

- Vink, T.J., W. Walrave, J.L.C. Daams, P.C. Baarslag and J.E.A.M. Van Den Meerakker, 1995. On the homogeneity of sputter-deposited ITO films Part I; Stress and microstructure. *Thin Solid Films*, 266: 145-151.
- Vora, A., J. Gwamuri, N. Pala, A. Kulkarni, J.M. Pearce and D.O. Guney, 2014. Exchanging ohmic losses in metamaterial absorbers with useful optical absorption for photovoltaics. *Sci. Rep.*, 4: 1-13.
- Zaier, A., A. Meftah, A.Y. Jaber, A.A. Abdelaziz and M.S. Aida, 2015. Annealing effects on the structural, electrical and optical properties of ZnO thin films prepared by thermal evaporation technique. *J. King Saud Univ. Sci.*, 27: 356-360.
- Zeng, Z., K. Wang, Z. Zhang, J. Chen and W. Zhou, 2008. The detection of H<sub>2</sub>S at room temperature by using individual Indium Oxide nanowire transistors. *Nanotechnol.*, 20: 1-4.